THE JOURNAL OF PHYSICAL CHEMISTRY B

Article

pubs.acs.org/JPCB

Correlations between Conjugation Length, Macromolecular Dynamics, and Photophysics of Phenylene-Vinylene/Aliphatic Multiblock Copolymers

O. D. Bernardinelli,[†] S. M. Cassemiro,[‡] L. A. O. Nunes,[†] T. D. Z. Atvars,[§] L. Akcelrud,*[,‡] and E. R. deAzevedo*[,†]

[†]Instituto de Física de São Carlos, Universidade de São Paulo, Caixa Postal 369, CEP 13560-970, São Carlos, São Paulo, Brazil

[‡]Paulo Scarpa Polymer Laboratory, Federal University of Parana, CP 19044, CEP 81531-990, Curitiba, PR, Brazil

[§]Chemistry Institute, State University of Campinas (Unicamp), Caixa Postal 6154, CEP 13084-971, Campinas, SP, Brazil

ABSTRACT: This work reports a detailed spectroscopy study of a series of multiblock conjugated nonconjugated copolymers built by *p*-phenylene vinylene type units (PV) and octamethylene spacers, namely, poly(1,8-octanedioxy-2,6-dimethoxy-1,4-phenylene-1,2-ethenylene) (LaPPS18). The relative proportions of the PV and aliphatic segments were estimated on the basis of solid-state NMR and Raman spectroscopy. The overall structure was characterized by wide angle X-ray diffraction; ^{1}H wide-line dipolar chemical shift correlation (DIPSHIFT), and centerband-only detection of exchange (CODEX) NMR data, that together with glass transition temperatures allowed us to identify the groups involved in the molecular dynamics. These different structural properties were used to explain the photoluminescence properties in terms of peak position and spectral profile

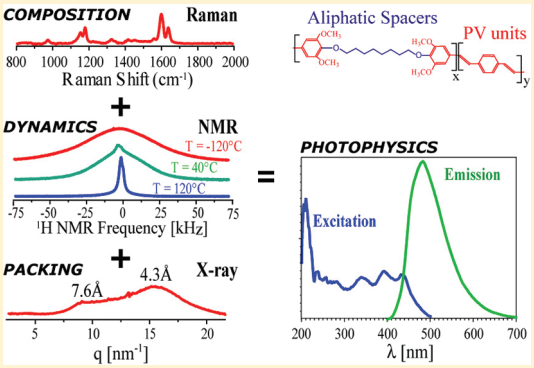

1. INTRODUCTION

The growing interest in electroluminescent polymers is due to the promising technological applications, such as displays in many electronic components, and the scientific interest in this class of materials as well. Some of the electroluminescent polymers are fully conjugated main chains, but usually, due to structural defects, the effective length of conjugation is statistically distributed, leading to the formation of chromophores with different energy barriers (gaps). In particular, poly(*p*-phenylene−vinylene) derivatives are conjugated polymers with different band gaps depending on the molecular structure, conjugation lengths, and lateral substituents.[1−4] In general, in the mixture of chromophores with different band gaps, those with small energy barriers are the emitting species, because of the very efficient intrachain energy migration and interchain energy transfer processes.[5−7] There are some strategies to control the intrachain processes, and in general, they use the confinement of the lumophores by the inclusion of torsion in the aromatic ring (as in ortho or meta substitution) and insertion of side chains that interrupt the conjugation by steric interactions or by the attachment of nonconjugated groups.[8−10] Some of these strategies (breaking of the planarity) also interfere with the interchain energy transfer process. In addition, chain structures with meta-links also reduce interchain interactions that often limit the efficiency of photoluminescence.[11,12] Another effective method of lumophore confinement involves the intercalation of a well-defined aliphatic spacer among conjugated lumophores, forming multiblock conjugated-nonconjugated chains. Copolymers with long aliphatic spacers may result in devices with high efficiency.[13,14] Depending of the chemical structure, the multiblock conjugated−nonconjugated copolymers are soluble and homogeneous in terms of conjugation length and can be designed to emit in a specific range of the visible spectrum.[1,13] In addition to the control of the energy band gap, and thus the color of the emission, the presence of the aliphatic groups breaks the planarity, reducing energy migration and energy transfer processes, and consequently, an increase of the PL efficiency is observed.[15] Moreover, the random interruption of conjugation by saturated groups of the prototypical electroluminescent polymer of *p*-phenylene−vinylene (PPV) increased the device efficiency by 30 times compared with the case of the fully conjugated PPV device.[16] These effects are attributed to reduced interchain interaction with the interruption of conjugation, resulting in high quantum efficiency of photo- and electroluminescence. This method was used to prepare well-defined multiblock polymers of the conjugated−nonconjugated type studied here, built with octamethylene blocks interspersed in the PV blocks. This structure was the first soluble blue emitter (465 nm) reported.[17,18] Three multiblock conjugated−nonconjugated copolymers were prepared using PV segments interspersed among octamethylene spacers, resulting in copolymers with

Received: December 6, 2011
Revised: March 30, 2012
Published: April 24, 2012

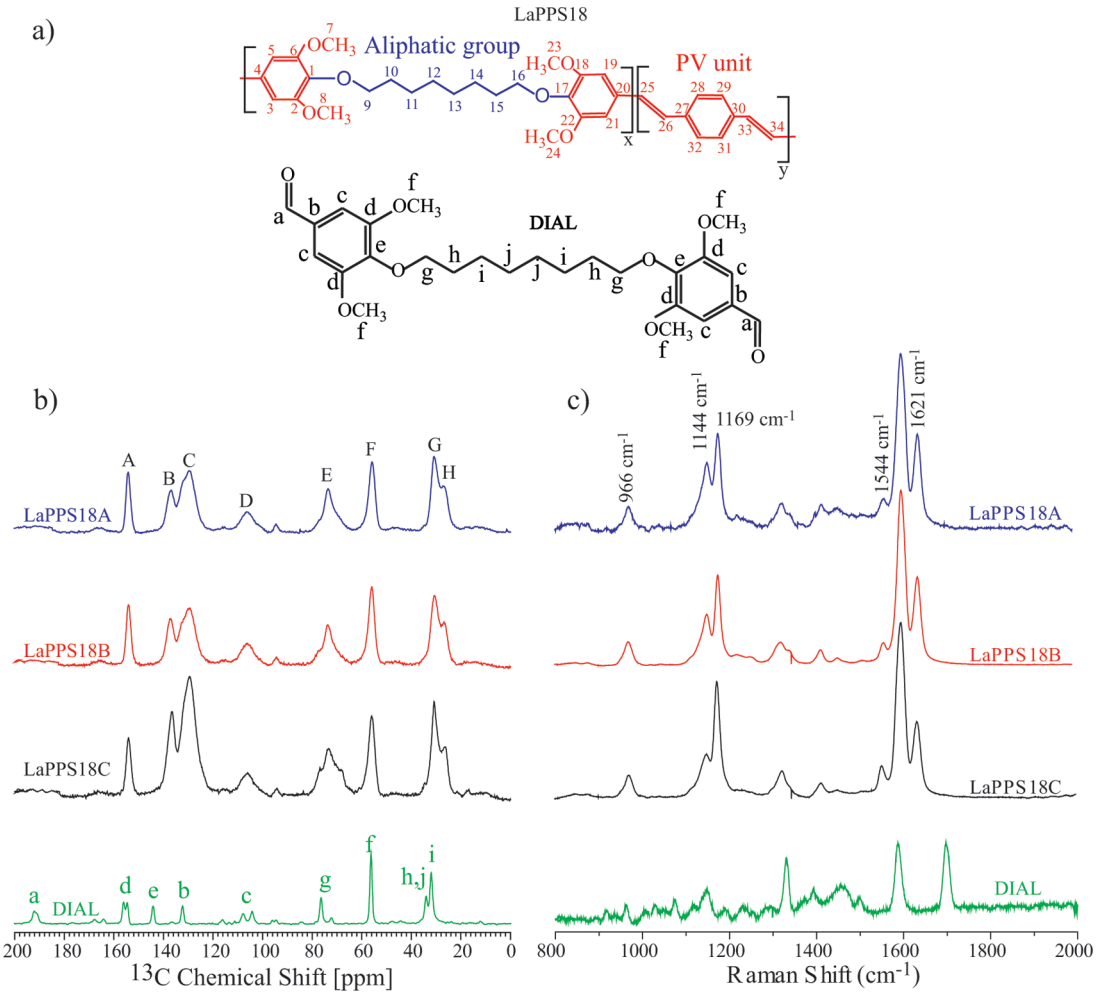

Figure 1. (a) Illustration of the chemical structures of LaPPS18 and of the precursor DIAL. (b) ^{13}C CPMAS NMR with the following assignments A, carbons 2,6,18,22; B, carbons 1,4,17,20,27,30; C, carbons 25,26,28,29,31,32,33,34; D, carbons 3,5,19,21; E, carbons 9,16; F, carbons 7,8,23,24; G, carbons 10,11,14,15; H, carbons 12,13. (c) Raman scattering spectra of the copolymers LaPPS18A, LaPPS18B, LaPPS18C, and the DIAL precursor. The main bands are indicated.

different structural and optical properties. The structural characterization was based on NMR and Raman data, which along with overall structure results from wide angle X-ray diffraction (WAXS) were correlated with macromolecular dynamics and photoluminescence mechanisms

2. METHOD AND MATERIALS

Materials. All experiments were carried out in powder samples, and the detailed procedures used in the synthesis of the copolymers were previously reported.[17,18] The materials used in the present study were 1,2-bis(4-formyl-2,6-dimethoxyphenoxy) octane (DIAL); [poly(1,8-octanedioxy-2,6-dimethoxy-1,4-phenylene-1,2-ethenylene)] copolymer, labeled as LaPPS18A ($\bar{M}_n$ = 29000 kg/mol, polydispersity = 1.4, T_g = 31.8 °C); LaPPS18B ($\bar{M}_n$ = 3200 kg/mol, polydispersity = 3.2, T_g = 45.5 °C); and LaPPS18C ($\bar{M}_n$ = 2600 kg/mol, polydispersity = 4.0, T_g = 58.6 °C). Because all dynamical properties are affected by the sample preparation, the experiments were performed using the same batch and samples maintained under the same conditions.

Methods. NMR experiments were performed using a VARIAN INOVA spectrometer at ^{13}C and ^{1}H frequencies of 100.5 and 400.0 MHz, respectively. A VARIAN 7-mm MAS double-resonance probe head with variable temperature (VT) was used. The spinning frequencies, varying between 4 and 6 kHz, were controlled by a VARIAN pneumatic system that ensures a rotation stability of ~2 Hz. Typical $\pi/2$ pulse lengths of 3.5 and 4.5 μs were applied for ^{13}C and ^{1}H, respectively. Time proportional phase modulated (TPPM) proton decoupling was used with a field strength of 60 kHz, a cross-polarization time of 1 ms, and recycle delays of 2 s. The amplitude and rates of slow molecular motions were investigated using the center-band-only detection of exchange (CODEX) technique[19,20] using a constant time scheme named constant time recoupling of the anisotropies (CONTRA)[21,22] with mixing time t_m of 300 ms and maximum evolution times ($4Nt_r$) of 800 μs. The temperature dependence of the C−H dipolar coupling was measured using the dipolar-chemical shift correlation (DIPSHIFT) technique,[23] where H−H homonuclear decoupling was achieved by the phase-modulated Lee−Goldburg (PMLG) sequence, using field strengths of approximately 60 kHz. The molecular dynamics of the copolymers was investigated using solid-state nuclear magnetic resonance. To obtain more details about the dynamic processes and their relationships with the molecular structure and composition, more specific methods needed to be used. Particularly since the ^{1}H NMR lines of LaPPS18B and LaPPS18C presented similar temperature dependence, not

dx.doi.org/10.1021/jp2117517 | J. Phys. Chem. B 2012, 116, 5993−6002

much could be concluded from these experiments. Thus, identifying which are the molecular segments responsible for the molecular relaxations and estimating dynamic parameters such as motion amplitudes and rates might be useful in the understanding of the differences in the molecular properties of these two samples. This can be inferred using more advanced NMR methods. Thus, the NMR techniques DIPSHIFT and CONTRA were applied to estimate the rates, amplitudes, and activation energies of the dynamic processes observed in the ^{1}H NMR experiments.

Raman spectra were recorded using a Titanium/Safire laser emitting at 790.1 nm, a Spex 1877 Triple Spectrometer, and a Jobin Yvon Spectrum-One cryogenic CCD detector. The spectra were acquired in the 800−2000 cm^{-1} range.

The model compound DIAL was used as a reference assignment for the NMR and RAMAN spectra.

Fluorescence spectroscopy experiments were performed using the 325 nm line of a HeCd laser, a Thermo Jarrell-Ash (30 cm) monochromator, and a Hamamatsu R928 photomultiplier. The 650 nm second harmonic was eliminated with a 350 nm high pass filter. Photoluminescence excitation spectra were acquired in a Perkin Almer Lambda 900 spectophotometer. The powder samples were deposited on quartz plates, and the excitation wavelenghts varied from 200 to 600 nm. The emission wavelenghts were 550 nm for LAPPS18A and 600 nm for LAPPS18B and C, corresponding to the maximum of the photoluminescence spectrum of each copolymer.

WAXS experiments were performed at the SAXS1 beamline of the Brazilian Synchrotron Light Laboratory (LNLS) . The wavelength used was 1.48 Å, and the sample detector distance was approximately 189.6 mm. The experiment was performed in powder samples. The sample scattering was registered using a two-dimensional MAR-CCD detector with 5 min of data acquisition. Average radial intensity profiles were obtained by integrating an arbitrary 5° angular sector. Intensities were normalized by the integrated intensity incident on the sample during the exposure and by sample absorption. Parasitic scattering was subtracted from each pattern.

3. RESULTS

To correlate chemical structure and composition with physical properties in a consistent way, a thorough molecular characterization was performed. The copolymer samples with PV segments of different length and content were labeled LaPPS18A, LaPPS18B, and LaPPS18C and are illustrated in Figure 1a. The differences in molar masses were accounted for by the decrease in solubility of the formed polymer in the reaction medium with the progressive incorporation of PV units.[17]

LaPPS18C had lower molar mass, higher polydispersity, and higher glass transition temperature as compared to LaPPS18A. On the contrary, LaPPS18B has approximately the same molar mass but lower T_g compared to LaPPS18C.

These results may suggest that LaPPS18C has some structural properties giving higher probability of aggregation in the solid state. The copolymers structure was addressed using Raman spectroscopy and several methodologies of solid state NMR to generate structural parameters to explain the physical data obtained.

Chemical Structure and Composition. In copolymers the final composition is often different from that of the reaction medium due to differences in reactivity and relative amounts of the reacting species near the propagation end of the growing chain. To achieve the exact composition of each copolymer in terms of the ratio between the aliphatic and PV segments, solid-state CPMAS and Raman experiments were performed.

The CPMAS solid-state NMR spectra of the samples are shown in Figure 1b. The assignments of the lines to the specific carbons, numbered according to the chemical structure of Figure 1a, are shown in the figure caption. These assignments were based on the typical chemical shift values, from the previous PPV spectra reported in refs 20 and 24 and also on the spectra of the precursor DIAL, shown at the bottom of Figure 1b. The exact ratio between aliphatic (represented as x) and PV (represented as y) units may vary considerably from that expected from the chemical synthesis, as noted. Thus, to characterize the composition of the solid copolymers, CPMAS spectra of each sample were run. Despite the fact that CPMAS is known to be a nonquantitative method, we have shown recently[25] for a similar copolymer that the combination of dipolar dephased, CPMAS with a radiofrequency ramp and proper spectral treatment allows a good estimation and quantification of the copolymer constitution,[25] which was determined for the full series of LaPPS18. Hence, the same method was applied here to extract the number of the PV units. The line assigned as A accounts for the $4x$ O-aromatic carbons in the linker group (see Figure 1), while line B arises from the $2y$ quaternary carbons in the phenylene groups and the $4x$ quaternary carbons in the linker. Ramped CPMAS is a semiquantitative experiment in the sense that the comparison between the integrated line intensities of carbons of the same type (nonprotonated for example) allows an estimation about the number of carbons that account for each line.[25] Thus, as lines A and B arise only from nonprotonated carbons, their intensity ratio allowed the determination of the number of PV units in each copolymer, that is, the length of the conjugated segment.

Figure 1c shows the Raman spectra of the three copolymers. By direct comparison of the spectra of Figure 1c with the poly(p-phenylene−vinylene) (PPV) spectra reported in the literature,[26] one can assign most of the bands to the PV segments, except for the bands at 1144 and 1330 cm^{-1}. To identify these two extra bands, the Raman spectra of the precursor (DIAL) was also acquired, shown in Figure 1c (bottom). The DIAL spectrum contains the main bands at 1330, 1580, and 1700 cm^{-1}. This allows the direct assignment of the 1330 cm^{-1} band in the copolymers spectra to some internal mode of the linker ring. The dial band at 1580 cm^{-1} coincides with a PV band, but the band at 1700 cm^{-1} does not appear in the copolymers spectra, which otherwise show a strong band 1144 cm^{-1}, that has a correspondent band on the DIAL spectra. This suggests that the dial band at 1700 cm^{-1} is, probably, due to a mode associated with the COH terminal groups of the DIAL molecule, which disappears with the copolymerization. In this sense, the intensity ratio between the band at 1144 cm^{-1}, associated with the linker bond, and that at 1169 cm^{-1}, associated with the phenylene C−C stretching and CH bending,[26−28] is proportional to the PV/aliphatic segments in the copolymers. Therefore, the number of PV units in the samples can also be obtained from this ratio. The results are shown in Table 1 and are in good agreement with those obtained by NMR.

The collected data from both NMR and Raman measurements showed that LaPPS18A and LaPPS18B have about the same average number of PV units per number of aliphatic groups while for LaPPS18C the number of PV units is about

Table 1. Relative Number of PV Units Per Number of Aliphatic Groups in the LaPPS18 Copolymers as Determined by Solid-State NMR and Raman Spectroscopy

copolymer	avg no. of PV units (from CPMAS)	avg no. of PV units (from Raman)
LaPPS18A	1.5 ± 0.2	1.5 ± 0.2
LaPPS18B	1.6 ± 0.2	1.8 ± 0.2
LaPPS18C	3.0 ± 0.2	2.7 ± 0.2

two times higher. It is noteworthy that LaPPS18A and LaPPS18B have quite different molar masses ($\bar{M}_n$ = 29000 and 3200 kg mol^{-1}, respectively) and polydispersities (1.4 and 3.2, respectively) in spite of having about the same ratio of PV and aliphatic segments. These results indicate that the physical properties seem to be much more controlled by the molar mass than by the segmental ratio. To get additional structural and solid state morphological information, another set of experiments was performed, as follows.

Chain Length Distribution, Packing, and Molecular Aggregation. In the results presented so far, the Raman spectra were used only to confirm the NMR results about the copolymer compositions. However, there are several experimental and theoretical works showing that Raman spectra also bring information about the degree of conjugation extension of the PV units. In ref 27, it was shown that the band intensity ratio I_{1169}/I_{1621} increases with the number of phenyl rings, which again allows us to conclude that the number of PV units, i.e. the conjugation extension, is higher for LaPPS18C and about the same for LaPPS18A and LaPPS18B, as shown in Figure 1c. The band at 966 cm^{-1} attributed to torsion of CH *trans*-vinylene out of plane (vinylene warpping) is also informative in terms of the molecular arrangement. This band is not expected for a fully planar configuration of the phenyl ring;[28] consequently, its presence can be interpreted as evidence of deviation from a fully planar configuration of the phenyl rings, which is indeed expected due to the presence of the aliphatic spacer groups.

Wide angle X-ray scattering measurements were also conducted to obtain information about the copolymer molecular arrangements. The results are shown in Figure 2. As can be observed, there is no sharp reflection in the diffractograms, which shows that there are no long-range crystalline domains in the copolymers. The patterns resemble those measured for noncrystalline conjugated polymers, for example, side-chain branched PPV derivatives,[29] but without the typical strong reflection corresponding to a Bragg distance of ~15 Å (parallel packing of the phenyl rings spaced by the lateral chain). The broad peak corresponding to a distance of ~4.5 Å, usually associated with packing parallel (face to face) to the phenyl rings, shows that molecular aggregation is present in all the copolymers. The reflection at ~7.6 Å that is well-defined for LaPPS18A is associated with the length of the PV units.

The diffractogram of LaPPS18C shows a sharper peak at ~4.3 Å, which was interpreted as a result of the onset of its crystallization, showing that, with an increase of the PV units, nanocrystalline domains start to be formed in the copolymers. Another feature that can be noticed in Figure 2 is that the pattern of LaPPS18B is more spread over the q^{-1} range than that of LaPPS18A. This shows that, despite having about the same average number and size of conjugated PV segments, the LaPP18B aggregates have higher size distribution and molecular disorder as compared with LaPP18A. This in

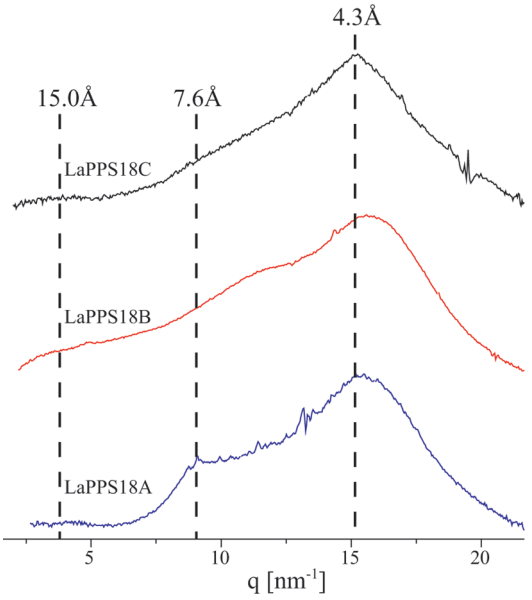

Figure 2. Wide angle X-ray scattering patterns of LAPP18 copolymers in solid powder.

agreement with the polymer polydispersity, but it brings the additional information that the lower molar mass in combination with higher relative ratio of PV segments facilitate the formation of the molecular aggregates, at least in the nanoscale domains. Moreover, the correlation between the WAXS and the polydispersity data suggested that the difference among the polydispersity values is mostly associated with the size distribution of the PV units.

The WAXS results, along with the molar masses and the relative content of PV segments, lead to the conclusion that LaPPS18C seems to be a more ordered material, indicating that the combination of low molar mass and high relative content of PV units imparts higher ability to order, and consequently, higher T_g. To confirm this partial conclusion, experiments using molecular dynamics were performed.

Molecular Dynamics. To identify the dynamic processes, ^{1}H wide-line nuclear magnetic resonance spectra were acquired as a function of temperature. As a result of the orientation dependence of the dipolar H−H coupling that dominates the ^{1}H spectrum, the temperature dependence of the solid-state ^{1}H line can give information about the presence of chain dynamics in the microsecond to millisecond time scale. If the molecular motions are much slower than the H−H dipolar coupling, known as the rigid limit regime, the ^{1}H solid-state spectrum is a broad Gaussian line, which is temperature independent. As the frequency of the molecular motions becomes comparable to the H−H dipolar coupling (typically ~40 kHz), the molecular motion starts averaging the dipolar interaction, the so-called intermediate limit regime, producing a line narrowing, which is frequently referred to as motional narrowing. As the motion rate becomes higher than the strength of the H−H dipolar interaction, the fast limit regime, the dipolar interaction decreases to an average value, which is dependent on the geometric characteristics of the molecular motions. In systems where the molecular dynamics is similar for all chemical moieties, the ^{1}H spectrum can be simulated and compared with the experimental one to obtain the rate and, to some extent, the geometry of the molecular motion. However, the LaPPS18 copolymers possibly exhibit multiple motional modes occurring

dx.doi.org/10.1021/jp2117517 | J. Phys. Chem. B 2012, 116, 5993−6002

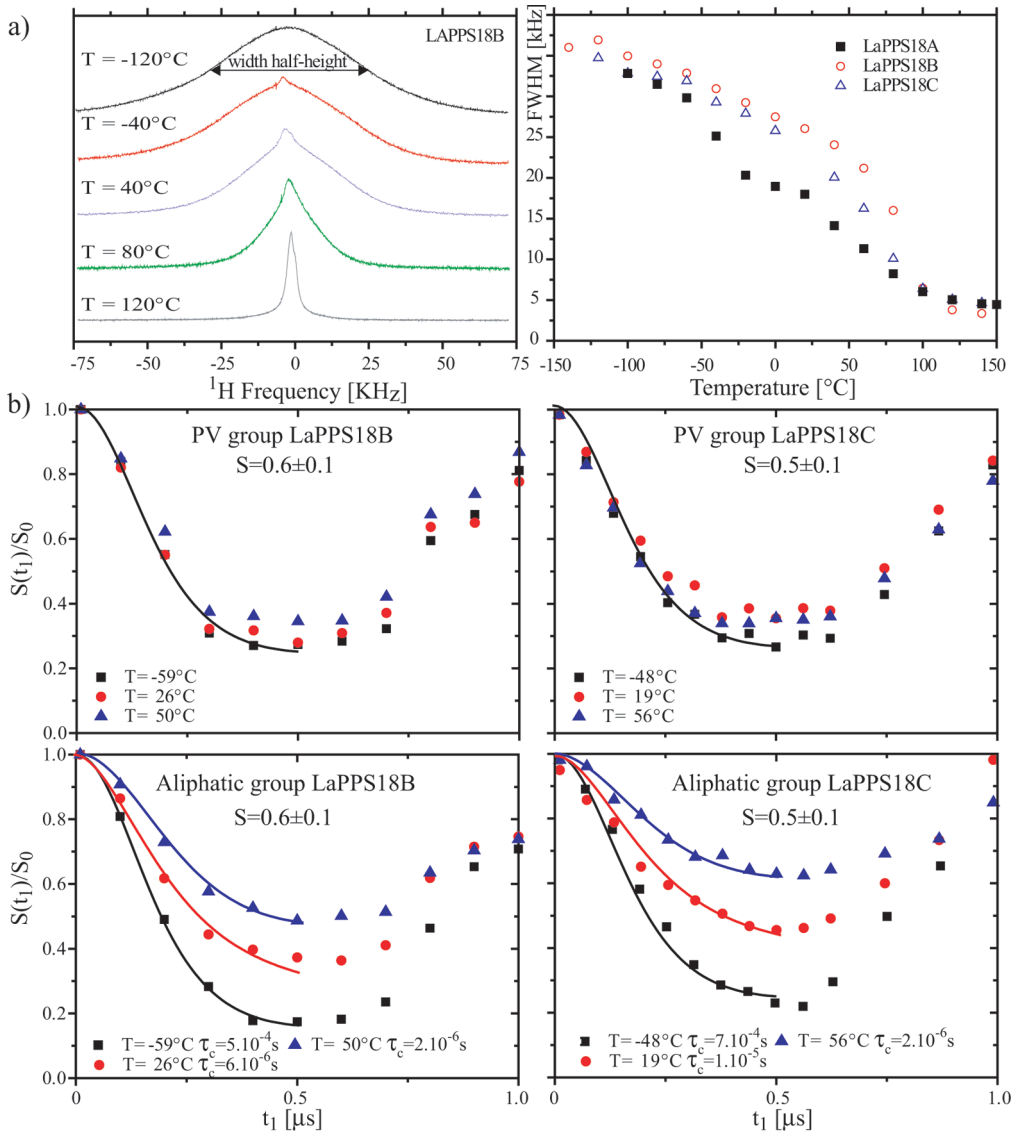

Figure 3. (a) ^{1}H wide-line spectra of sample LaPPS18A as a function of temperature (left). ^{1}H line width (full width at half-maximum (fwhm)) as a function of temperature (right). (b) $S(t_1)/S(0)$ curves obtained from the integral intensity of line C in the CPMAS spectra presented in Figure 1 for the samples LaPPS18B and LaPPS18C as a function of temperature. (c) $S(t_1)/S(0)$ curves obtained from the integral intensities of lines G and H in the CPMAS spectra for samples LaPPS18B and LaPPS18C as a function of temperature.

in distinct molecular branches, so the quantification of the molecular dynamics parameters using only the ^{1}H NMR spectrum becomes dubious. Even in these cases, the observation of the spectra as a function of temperature is useful, since the typical line narrowing permits determination of the temperature that characterizes the onset of the motions on the microsecond time scale. This is shown in Figure 3a (left), which presents the ^{1}H wide-line spectra of sample LaPPS18A as a function of temperature. The appearance of sharp peaks is evident in all samples, showing the onset of a molecular dynamic process with rates on the order of kilohertz. Figure 3a (right) also shows the plot of the ^{1}H line width (full width at half-maximum (fwhm)) as a function of temperature. In all samples, two line narrowing temperatures can be distinguished. As can be seen, most evidently in sample LaPPS18A, at low temperatures the ^{1}H line width is about 50 kHz, narrowing first to about 20 kHz and then to 5 kHz at higher temperatures. This indicates that all samples exhibit two dynamic transitions, or molecular relaxations, which will be referred to as α' (at lower temperatures) and α (at higher temperatures). The line narrowing associated with the α' relaxation is visibly more abrupt in sample LaPPS18A. This suggests smaller motion heterogeneity in this sample, which is typical of a more amorphous local environment of the aliphatic chains.

The DIPSHIFT method provides a measurement of the ^{13}C−H magnetic dipolar coupling of each chemical group. This is done by measuring the dependence of the signal amplitude (each line on the CPMAS spectrum) with an evolution period (t_1), where the nuclear spins evolve under the action of the CH magnetic dipolar coupling, producing a curve $S(t_1)/S(0)$, that depends on the dipolar coupling strength. Motions with rates between 10^3 and 10^7 Hz average the ^{13}C−H coupling,[30,31] resulting in $S(t_1)/S(0)$ curves that depend on the presence of molecular motions. Figure 3b shows $S(t_1)/S(0)$ curves obtained from the integral intensity of line C in the CPMAS spectra presented in Figure 1 for the samples LaPPS18B and LaPPS18C. As can be noticed, in the −60 to 60 °C temperature range, the $S(t_1)/S(0)$ curve does not show a temperature

dx.doi.org/10.1021/jp2117517 | J. Phys. Chem. B 2012, 116, 5993−6002

dependence, which stands for the rigidity of the PV chains in both samples. In contrast, in lines G and H, $S(t_1)/S(0)$ (Figure 3c, which accounts for the CH_2 aliphatic carbons) shows an evident reduction of the C−H dipolar coupling as a function of temperature. Therefore, the results depicted in Figure 3b and c indicate that the molecular motion with rates between 10^3 and 10^6 Hz is restricted to the CH_2 aliphatic groups, with the PV units being rigid at this frequency scale and in this temperature range. Moreover, it is possible to observe that the DIPSHIFT curves at the highest temperature are slightly distinct for the two samples. In these cases, the motion is already in the so-called fast regime, so the curves do not depend on the correlation time but only on the value of the averaged dipolar coupling, which can be associated with the motion geometry. In fact, by simulating the fast limit DIPSHIFT curve, one can estimate the residual dipolar coupling, which can then be related to the motional order parameter S, considering a model of reorientation in a cone.[32] Using this approach, we have estimated the order parameter for the two samples, obtaining S = 0.6 and 0.5 for LaPPS18B and LaPPS18C, respectively. The lower order parameter for LaPPS18C indicates that in this case the motions of the aliphatic chains are slightly more restricted, which can be associated with a more densely packed structure, in agreement with the behavior observed in the WAXS results. The correlation times of the motion can be estimated via DIPSHIFT by fitting the experimental results using the formula based on the so-called Anderson−Weiss (AW) approximation.[33,34] The AW approximation considers a Gaussian distribution of local dipolar fields and diffusive anisotropic motions (diffusion of a CH bond in a cone), so that the correlation times are the unique fitting parameter. In ref 35 it was shown that for DIPSHIFT evolution times shorter than half of the rotation period (t_r) the AW fit can be used even for nondiffusive motions. Thus, Figure 3c also shows the DIPSHIFT curves corresponding to the integral intensity of lines G and H in the CPMAS spectra of samples LaPPS18B and LaPPS18C for evolution times from 0 to 100 μs (0 to $t_r/2$). The fits using the AW fit are also shown together with the correlation times extracted for each temperature. From an Arrhenius plot of the correlation times as a function of temperature (not shown), an activation energy of about 30 kJ/mol was calculated for both samples, which is expected since the aliphatic chains have the same chemical structure.

The DIPSHIFT results showed the absence of 10^3−10^6 Hz main chain motions in the −60 to 60 °C temperature range. However, from the ^{1}H line width measurements, one should expect this kind of motions to start at higher temperature. However, to probe that by DIPSHIFT one should carry out the measurement at temperatures above 80 °C, which is in the borderline of the maximum temperature achieved in the MAS probe. Hence, it is more interesting to use a technique capable of probing slower motions, for example in the hertz to kilohertz frequency scale. This can be done with high resolution using the so-called centerband-only detection of exchange (CODEX).[19,20] To achieve a better performance, we actually used a CODEX variant named as CONTRA, from constant time recoupling of the anysotropies.[22] This experiment is capable of probing molecular motions with rates between hertz and kilohertz,[22] providing reliable information about the amplitude of the molecular motions. The experiment detects the signal reduction due to changes in the orientation-dependent chemical-shift frequencies (encoded by an evolution period with duration of $t_1 = s*2\text{tr}$, s = 0, ..., 1) that take place during a mixing time (t_m),[22] usually on the order of hundreds of milliseconds. Quantification is performed by taking line intensities of the NMR spectrum obtained after applying the pulse sequence, S, and subtracting from the corresponding intensities obtained in a reference spectrum, S_0. The reference spectrum is acquired in such a way that no molecular motion effects are encoded, but it has the same intensity reduction due to relaxation effects as the S spectra. The intensity difference obtained for each individual line in the spectra is then normalized $\Delta S/S_0 = (S_0 - S)/S_0$ and plotted as a function of t_m or t_1, giving rise to a curve that depends on the correlation times (t_m dependence) or on the reorientation angle (t_1 dependence) of the slow molecular motion. Besides, for $t_m \gg \tau_c$ and $t_1 \gg 1/\delta$ the value of $\Delta S/S_0 = (S_0 - S)/S_0$ is proportional to the fraction of molecular segments that execute reorientation in the millisecond to seconds time scale. This makes it possible to obtain information about the motion heterogeneities directly from the curve obtained by plotting the $\Delta S/S_0$ intensity as a function of temperature acquired with ($t_1 \gg 1/\delta$). This is so because if the motion heterogeneity (distribution of correlation times) is small, there will be a temperature where all the molecules execute motion in the frequency range detectable by CODEX, so the $\Delta S/S_0$ intensity will achieve a maximum that will depend only on the motion geometry (for example, if the motion is isotropic, $\Delta S/S_0$ becomes equal to the unit). On the other hand, if the width of the distribution of correlation times exceeds the sensitivity window of the CODEX, part of the molecules will always be moving slower or faster than the CODEX detection window (∼1 ms to ∼1 s) and will not contribute to $\Delta S/S_0$ intensity. Thus, the maximum achieved for the $\Delta S/S_0$ intensity as a function of temperature will decrease (again, in the case of isotropic motion, it will be smaller than the unity). Apart from that, the temperature where the maximum of $\Delta S/S_0$ occurs is dictated by the apparent activation energy of the motions, being shifted to higher temperatures for higher activation energies. Strictly speaking, to characterize the motion geometry using a $\Delta S/S_0$ vs t_1 curve, it is necessary to know very well the principal values and the principal axis orientation of the chemical shift anisotropy (CSA) tensor for the carbons which are being used to probe the molecular motions. While the CSA principal values can be easily obtained using the so-called Herzfeld and Berger analysis,[36] the determination of the principal axis orientation relative to the molecule is more tricky and, when possible, requires extensive multidimensional experiments.[23,37] Hence, instead of trying to accomplish a profound characterization of the motion geometry, we focus on the general features concerning the backbone motions, for example, if the motions around T_g are isotropic or anisotropic. To achieve that, a rough estimation of the PAS orientation suffices, particularly for isotropic motions. Thus, in our simulations the principal axis corresponding to the principal value σ_{zz} (z-axis) was assumed to be normal to the phenylene ring plane. The x-axis, corresponding to σ_{xx}, was considered to be along the bond between the aromatic quaternary carbon and the vinylene carbon, and the y-axis, corresponding to σ_{yy}, is in the ring plane, 90° from the x-axis. σ_{xx} = 71 ppm, σ_{yy} = 168 ppm, and σ_{zz} = 220 ppm were obtained from a Herzfeld and Berger analysis of the spinning side bands of the peaks corresponding to lines A, B, and C. Once these values were known, the $\Delta S/S_0$ vs t_1 curves were simulated considering random jumps between 300 sites distributed in a sphere surface to mimic isotropic motions.[38]

dx.doi.org/10.1021/jp2117517 | J. Phys. Chem. B 2012, 116, 5993−6002

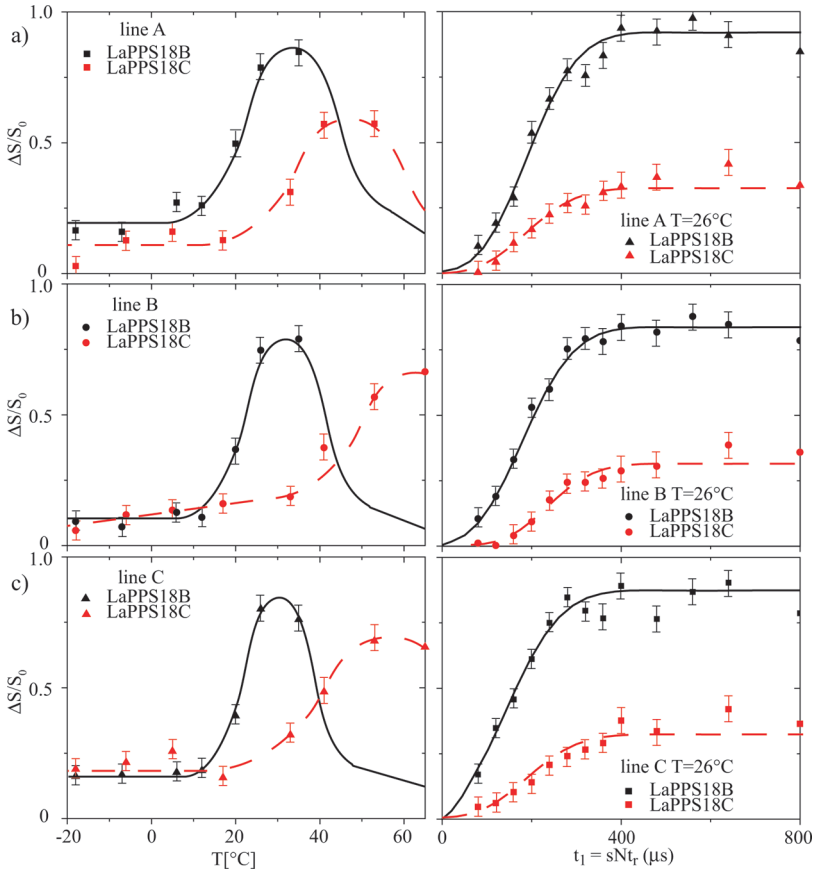

Figure 4. $\Delta S/S_0$ CONTRA intensities ($t_1 \gg 1/\delta$) as a function of temperature (left) and as a function of t_1 (right): (a) line A, (b) line B, and (c) line C.

For that, a home-built FORTRAN program was used; see ref 39 for details.

Figure 4 (left) show the $\Delta S/S_0$ CONTRA intensities ($t_1 \gg 1/\delta$) as a function of temperature. As already mentioned, the maximum achieved in these curves is dictated by the width of the correlation time distribution of the molecular motion, while the temperature position depends on the facility of activation by the temperature of the molecular motion (apparent activation energy). In this sense, the results depicted in the left part of Figure 4 show that both the motional heterogeneity and the apparent activation energy are higher in LaPPS18C than in LaPPS18B. This is in agreement with the higher relative amount of PV units of LaPPS18C, which leads to a higher T_g. Moreover, the X-ray results may indicate the stiff nanoscale crystalline phase in LaPPS18C is not contributing to the slow molecular dynamics at T_g due to the decrease in the amount of mobile fraction in LaPPS18C, as observed in Figure 4 (right). This may also be operating in LaPPS18C, increasing the glass transition temperature. Hence, despite the different degrees of aggregation in the samples, the PPV chain length defines the onset of the main chain dynamics in the disordered PV regions. The fact that for sample LaPPS18B the curve reaches a maximum near the unity is an indicative that the motion involves many sites; that is, it is an isotropic type of motion. Note also that the curves for the different lines are mostly identical, which suggests that these slow motions are actually segmental rotations of the whole PV chain. Putting it all together, one can identify the α relaxation as a glass transition of the PV chains, which occurs at higher temperature for sample LaPPS18C than for LaPPS18B.

More specific information about the slow molecular dynamics was obtained from the $\Delta S/S_0$ CONTRA build up intensities as a function of t_1. The results are shown in Figure 4 (right), with all measurements being performed at room temperature (26 °C). As can be observed, the build ups are very similar for all analyzed lines, confirming that the backbone motions occur in all PV segments. Moreover, except for a decrease in the plateau value for LaPPS18C, the initial build ups of the curves are also similar between samples. This shows that the average reorientation angle during the backbone slow motions is similar for the two samples. The differences in the plateaus occur obviously because the differences between the temperatures were the molecular motions achieved on the millisecond and second time scales, as depicted in Figure 4 (right) and also because part of the LaPPS18C chain probably does not contribute to the slow backbone motions. The solid curves shown in Figure 4 are simulations considering random jumps between multisites distributed in a sphere to mimic the curve of isotropic motions.[39] The CSA principal values and orientations were those mentioned above. As discussed in detail in ref 39, $\Delta S/S_0$ vs t_1 values are not sufficiently sensitive to distinguish between different motional models for isotropic motions (random jumps, isotropic rotational diffusion, diffusion on a cone, etc.), but they can clearly distinguish between jumps between specific sites (N site jumps) and isotropic-like motions. Thus, despite the difficulties in knowing exactly the motion geometry, the very good agreements between the experimental and simulated curves again suggest that the slow backbone motion is a result of a glass transition in the disordered PV chains.

dx.doi.org/10.1021/jp2117517 | J. Phys. Chem. B 2012, 116, 5993–6002

Photoluminescence Spectra. To correlate the copolymer photoluminescence properties with morphology and molecular dynamics, excitation and emission (λ_{exc} = 325 nm) spectra were recorded at 27 °C (Figure 5). The LaPPS18A excitation

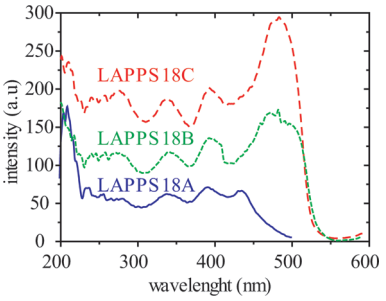

Figure 5. Excitation spectra for the LAPP18 samples. The emission wavelenghts were 550 nm for LAPPS18A and 600 nm for LAPPS18B and C, corresponding to the maximum of the photoluminescence spectrum of each copolymer.

spectrum (λ_{em} = 550 nm) is observed at higher energy and is composed by a well-defined vibronic progression with the lower energy band at 435 nm. These excitation bands are also observed for the other two copolymers (LaPPS18B and LaPPS18C), indicating that shorter conjugated segments are present in these three samples. Nevertheless, for LaPPS18B a lower energy band is also observed, centered at 480 nm, indicating that, in addition to the shorter segments, longer conjugated segments are also present. The LaPPS18C excitation spectrum displayed also a lower energy band in addition to the higher energy vibronic bands. However, when compared to the excitation spectrum of LaPPS18B, the lower energy band is broader and seems to present an excitonic splitting (peaks at 470 and 500 nm), which may be associated with the formation of aggregated species. The PL spectra are not mirror images of the excitation spectra (Figure 6), with much larger Stokes shifts. These results strongly indicate that even though the higher energy species have been excited, several types of faster mechanisms occurred after the excitation, such as energy migration and energy transfer processes toward some lower energy states. Thus, although the shorter segments or higher energy species are absorbing, the PL spectrum arises from lower energy species (from longer chain segments or aggregates).

Other remarkable observations are the variation of PL peak positions, whose maxima appear at room temperature (27 °C), and the peak profiles. For LaPPS18A the PL spectrum is broader and almost featureless at any temperature, while for LaPPS18B and LaPP18C the spectra are red-shifted and sharper and have the phonon replicas 0−0, 0−1, 0−2, and 0−3.[40] An attempt to deconvolute the spectrum and the corresponding wavelengths is shown in Figure 6. According to ref 40, the wavelengths for pristine PPV are 515, 540, 580, and 630 nm, which are in the same range as those found for LAPPS18B and LAPPS18C. This result also shows that although LaPPS18A and B have almost the same relative amount of PV segments, they are distributed in different ways: longer sequences appear for LaPPS18B compared to LaPPS18A, and the sequences for LaPSS18C are longer than those for LaPPS18B. What they have in common is a band around 470 nm which may be associated with isolated PV units.[18] The presence of this higher energy band may account

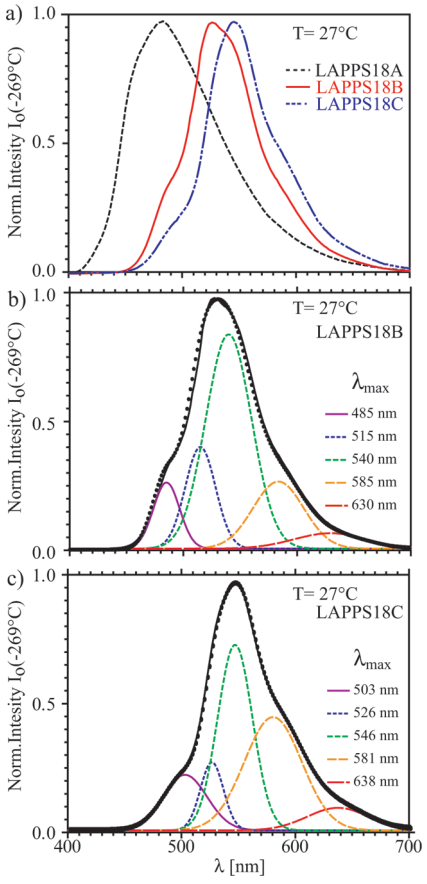

Figure 6. Steady-state photoluminescence spectra (PL) for samples (a) LaPPS18A, LaPPS18B, and LaPPS18C. (b) Gaussian deconvolution of the LaPPS18B PL spectra. (c) Same as part b for LaPPS18C.

for the emission of chains where exciton migration has not occurred for all of the PV segments[40,41] probably due to the intercalation by the flexible segments or because they are terminal groups.

The intensity profile of the vibronic replicas was not similar to that of PPV,[40] which cannot be explained by a simple analysis of the Huang−Rhys parameter. There are some possible reasons for that: since we are working with powder sample compressed in the form of thick samples, we cannot exclude the inner-filter effect, which may decrease artificially the relative intensity of the 0−0 band. In addition and probably with higher probability, aggregates are formed, and they are increasing the relative intensities of the lower energy bands. Indeed, for LaPPS18C this should be the case, since the data obtained by WAXS (the broader peak at 4.5 Å) suggested the presence of nanocrystalline domains dispersed into an amorphous and disordered matrix. With the present set of data, we are not able to discuss the type of the aggregates that has been formed. In general, H-aggregates have a sharper absorption (or excitation) band on the red-edge of the nonaggregate species. The spectral shift depends on the magnitude of the excitonic interactions.[42] If the interaction is very weak, the H-aggregate band is completely overlapped on the band or the nonaggregate species. When H-aggregates are formed, the Stokes shift of the PL spectrum is, in general, very small. On the other hand, the absorption bands for the J-aggregates are blue-shifted compared to that of the isolated species. The spectral splitting of the LaPPS18C excitation

dx.doi.org/10.1021/jp2117517 | J. Phys. Chem. B 2012, 116, 5993−6002

spectrum may suggest that J-aggregates are formed, which is consistent with the proposed nanocrystalline structures with the phenyl groups oriented in a face-to-face packing by WAXS. These structures should have a PL spectrum red-shifted with a large Stokes shift when compared to the case of the isolated molecules.

Relationship between Molecular Structure, Structural Dynamics, and Fluorescent Emission. X-ray, NMR, Raman, and PL measurements provided a quite complete picture about the differences in composition, structure, and molecular dynamics in LaPPS18 copolymers. From the fluorescence spectroscopy measurements, one can deduce that these differences have a direct and strong influence on the luminescent emission of the systems. Hence, in the following paragraphs we attempt to describe the possible correlations between the bulk emission and the molecular properties of the LaPPS18 copolymers.

Both NMR and Raman measurements show that the samples LaPPS18A and LaPPS18B have a similar average number of PV units (~1.5), while for LaPPS18C this number is higher (~3.0). The WAXS results showed that there is only crystallization in nanoscale domains and that in LaPPS18A there is an additional structure with a peak at 7.6 nm^{-1} absent in both LaPPS18B and LaPPS18C, which have lower molar masses. In addition, previous GPC measurements on the same samples revealed that the polydispersity of LaPPS18A is considerably smaller (~1.4) than those of LaPPS18B and C (~3.0−4.0). The glass transition temperatures also indicate that the LaPPS18A has simultaneously higher molar mass and lower T_g, indicating that this should be the more disordered material. Putting these data together, one can conclude that LaPPS18B and C form aggregated structures in nanoscale built up by the combination of longer PV sequences and lower molar mass chains as observed by WAXS.

The NMR measurements show two distinct dynamic processes at about −150 and 50 °C, which were associated with the aliphatic chain motions and the main chain, respectively. The low temperature process seems to be directly related to the change in the PL spectra observed above −80 °C (not shown). It is well established that molecular movements induce the appearance of nonradiative pathways that decrease the intensity of the PL bands. Besides, motion induced conformational disorder seems to be responsible for the broadening of the PL bands. However, in the present case, the motion occurs in the aliphatic chains, which do not contribute to the emission profile but may contribute to the decrease of the relative intensity as the temperature increases.[43,44] Indeed, the results show that, at the measured temperatures, the main chain remains mostly rigid, or only undergoes very slow reorientations. These results suggest that the decrease in the fluorescence and broadening of the PL bands can be induced by the onset of fluctuations in the local environment, creating a broader distribution of states.[4,10,40,45,46] Moreover, we also observed in Figure 6a a more complex spectral behavior for LaPSS18B and LaPSS18C than in LaPPS18A, probably due to the presence of more aggregated species. In general, a sharper PL spectrum is observed for emitting centers with a sharper distribution of state densities. Thus, to explain why a sample with higher polydispersity (LaPPS18C) presented sharper and red-shifted PL emission, with highest intensity peaks with lower energy, we must account for the aggregation. In other words, energy is transferred more efficiently from the higher energy segments to lower energy segments or to aggregates and the emission arises from a sharper distribution of species and states. Considering that the WAXS results showed that the aggregation is probably higher in the formers, one can take that as evidence that this effect is more pronounced in chains more exposed to the local environment, i.e., not deep inside the aggregated structures. Due to this complex behavior, the simulation of the temperature dependence of the spectral behavior was not further addressed.

4. CONCLUSIONS

The results presented clearly indicate that changes in the local packing and dynamics influence all of the dynamic properties, including the photoluminescent emission. The analysis of the results presented here provided a more systematic approach, since a series of copolymers with identical chemical units but different relative composition has been used. For example, we showed that the combination between lower molar mass and higher relative content of PV units (determined by both Raman spectroscopy and NMR data) may create a molecular arrangement that plays an important role on the polymer morphology, which in the WAXS experiments showed the nanoscale aggregates and, as a consequence, an increased glass transition. Thus, to avoid aggregation, a relatively larger amount of flexible conjugated spacers must be used, as observed for LaPPS18A. Also, these structural characteristics define the profile of the photoluminescence decay, the temperature dependence of these processes, and the dynamics of the segmental relaxation as shown by the NMR studies. Thus, control of the synthetic process by the intercalation of flexible segments between the PV sequences resulted in more flexible (lower glass transition) or more stiff copolymers (longer segments), which may be useful in flexible devices.

AUTHOR INFORMATION

Corresponding Author

*E-mail: azevedo@ifsc.usp.br; leni@ufpr.br.

Notes

The authors declare no competing financial interest.

ACKNOWLEDGMENTS

The authors are grateful to the Brazilian funding agencies FAPESP (Proc. number 2009/18354-8, 2009/14153-8) and CNPq (Proc. Number 579190/2008-0) and the National Institute of Electronic Organics (FAPESP/CNPq/MCT) for financial support and fellowships. The authors also acknowledge the Brazilian Synchrotron Light Laboratory (LNLS) research proposal SAXS1-9208.

REFERENCES

(1) Akcelrud, L. *Prog. Polym. Sci.* **2003**, *28*, 875−962.
(2) Nguyen, T. Q.; Doan, V.; Schwartz, B. J. *J. Chem. Phys.* **1999**, *110*, 4068−4078.
(3) Son, S.; Dodabalapur, A.; Lovinger, A. J.; Galvin, M. E. *Science* **1995**, *269*, 376−378.
(4) Hoffmann, S. T.; Bassler, H.; Kohler, A. *J. Phys. Chem. B* **2010**, *114*, 17037−17048.
(5) Traub, M. C.; Lakhwani, G.; Bolinger, J. C.; Vanden Bout, D.; Barbara, P. F. *J. Phys. Chem. B* **2011**, *115*, 9941−9947.
(6) Zucolotto, V.; Faceto, A. D.; Santos, F. R.; Mendonca, C. R.; Guimaraes, F. E. G.; Oliveira, O. N. *J. Phys. Chem. B* **2005**, *109*, 7063−7066.

(7) Claudio, G. C.; Bittner, E. R. *J. Phys. Chem. A* **2003**, *107*, 7092−7100.
(8) Yang, N. C.; Jeong, J. K.; Choi, S. J.; Rhee, T. H.; Suh, D. H. *Macromol. Rapid Commun.* **1999**, *20*, 586−590.
(9) Zhang, M.; Li, G. W.; Ma, Y. G.; Zhang, R. F.; Shen, J. C. *Mater. Lett.* **2003**, *57*, 4176−4181.
(10) Snedden, E. W.; Cury, L. A.; Bourdakos, K. N.; Monkman, A. P. *Chem. Phys. Lett.* **2010**, *490*, 76−79.
(11) Massuyeau, F.; Faulques, E.; Athalin, H.; Lefrant, S.; Duvail, J. L.; Wery, J.; Mulazzi, E.; Perego, R. *J. Chem. Phys.* **2009**, *130*, 124706.
(12) Wang, P.; Collison, C. J.; Rothberg, L. J. *J. Photochem. Photobiol., A* **2001**, *144*, 63−68.
(13) Yang, Z.; Hu, B.; Karasz, F. E. *J. Macromol. Sci., Pure Appl. Chem.* **1998**, *A35*, 233−247.
(14) Sun, R. G.; Wang, Y. Z.; Wang, D. K.; Zheng, Q. B.; Kyllo, E. M.; Gustafson, T. L.; Epstein, A. J. *Appl. Phys. Lett.* **2000**, *76*, 634−636.
(15) Kyllo, E. M.; Gustafson, T. L.; Wang, D. K.; Sun, R. G.; Epstein, A. J. *Synth. Met.* **2001**, *116*, 189−192.
(16) Burn, P. L.; Holmes, A. B.; Kraft, A.; Brown, A. R.; Bradley, D. D. C.; Friend, R. H. *Mater. Res. Soc. Symp. Proc.* **1992**, *247*, 647−654.
(17) Cassemiro, S. M.; Thomazi, F.; Roman, L. S.; Marletta, A.; Akcelrud, L. *Synth. Met.* **2009**, *159*, 1975−1982.
(18) Machado, A. M.; Neto, J. D. D.; Cossiello, R. F.; Atvars, T. D. Z.; Ding, L.; Karasz, F. E.; Akcelrud, L. *Polymer* **2005**, *46*, 2452−2460.
(19) deAzevedo, E. R.; Hu, W. G.; Bonagamba, T. J.; Schmidt-Rohr, K. *J. Am. Chem. Soc.* **1999**, *121*, 8411−8412.
(20) deAzevedo, E. R.; Franco, R. W. A.; Marletta, A.; Faria, R. M.; Bonagamba, T. J. *J. Chem. Phys.* **2003**, *119*, 2923−2934.
(21) Reichert, D.; Pascui, O.; Bonagamba, T. J.; deAzevedo, E. R.; Schmidt, A. *Chem. Phys. Lett.* **2003**, *380*, 583−588.
(22) Reichert, D.; Pascui, O.; Bonagamba, T. J.; Belton, P.; Schmidt, A.; Deazevedo, E. R. *J. Magn. Reson.* **2008**, *191*, 141−147.
(23) Munowitz, M.; Aue, W. P.; Griffin, R. G. *J. Chem. Phys.* **1982**, *77*, 1686−1689.
(24) Simpson, J. H.; Egger, N.; Masse, M. A.; Rice, D. M.; Karasz, F. E. *J Polym. Sci., Polym. Phys.* **1990**, *28*, 1859−1869.
(25) Nowacki, B.; DeAzevedo, E. R.; Akcelrud, L. *Polym. Test* **2011**, *30*, 342−347.
(26) Zeng, Q. G.; Ding, Z. J.; Tang, X. D.; Zhang, Z. M. *J. Lumin.* **2005**, *115*, 32−38.
(27) Mulazzi, E.; Ripamonti, A.; Wery, J.; Dulieu, B.; Lefrant, S. *Phys. Rev. B* **1999**, *60*, 16519−16525.
(28) Alimi, K.; Molinie, P.; Majdoub, M.; Bernede, J. C.; Fave, J. L.; Bouchriha, H.; Ghedira, M. *Eur. Polym. J.* **2001**, *37*, 781−787.
(29) Souza, A. A.; Cossiello, R. F.; Plivelic, T. S.; Mantovani, G. L.; Faria, G. C.; Atvars, T. D. Z.; Torriani, I. L.; Bonagamba, T. J.; Deazevedo, E. R. *Eur. Polym. J.* **2008**, *44*, 4063−4073.
(30) Deazevedo, E. R.; Saalwachter, K.; Pascui, O.; De Souza, A. A.; Bonagamba, T. J.; Reichert, D. *J. Chem. Phys.* **2008**, 128.
(31) Cobo, M. F.; Malinakova, K.; Reichert, D.; Saalwachter, K.; DeAzevedo, E. R. *Phys. Chem. Chem. Phys.* **2009**, *11*, 7036−7047.
(32) Lipari, G.; Szabo, A. *J. Am. Chem. Soc.* **1982**, *104*, 4546−4559.
(33) Hirschinger, J. *Solid State Nucl. Magn.* **2008**, *34*, 210−223.
(34) Hirschinger, J. *Concept Magn. Reson. A* **2006**, *28A*, 307−320.
(35) Faria, G. C.; Plivelic, T. S.; Cossiello, R. F.; Souza, A. A.; Atvars, T. D. Z.; Torriani, I. L.; deAzevedo, E. R. *J. Phys. Chem. B* **2009**, *113*, 11403−11413.
(36) Herzfeld, J.; Berger, A. E. *J. Chem. Phys.* **1980**, *73*, 6021−6030.
(37) Veeman, W. S. *Prog. Nucl. Magn. Reson. Spectrosc.* **1984**, *16*, 193−235.
(38) Schmidt-Rohr, K.; Spiess, H. W. *Multidimensional Solid-State NMR and Polymers*; Academic Press: San Diego, CA, 1994.
(39) Schmidt-Rohr, K.; deAzevedo, E. R.; Bonagamba, T. J. *Encycl. Nucl. Magn. Reson.* **2002**, *9*, 633−642.
(40) Zeng, Q. G.; Ding, Z. J. *J. Phys.: Condens. Matter* **2004**, *16*, 5171−5178.
(41) Bassler, H.; Schweitzer, B. *Acc. Chem. Res.* **1999**, *32*, 173−182.
(42) Kasha, M.; Rawls, H. R.; El-Bayoumi, M. A. *Pure Appl. Chem.* **1965**, *11*, 371.
(43) Abraham, S.; Atvars, T. D. Z.; Weiss, R. G. *J. Phys. Chem. B* **2010**, *114*, 12221−12233.
(44) Cossiello, R. F.; Kowalski, E.; Rodrigues, P. C.; Akcelrud, L.; Bloise, A. C.; deAzevedo, E. R.; Bonagamba, T. J.; Atvars, T. D. Z. *Macromolecules* **2005**, *38*, 925−932.
(45) Rumbles, G.; Samuel, I. D. W.; Collison, C. J.; Miller, P. F.; Moratti, S. C.; Holmes, A. B. *Synth. Met.* **1999**, *101*, 158−161.
(46) He, F.; Cheng, G.; Zhang, H. Q.; Zheng, Y.; Xie, Z. Q.; Yang, B.; Ma, Y. G.; Liu, S. Y.; Shen, J. C. *Chem. Commun.* **2003**, 2206−2207.